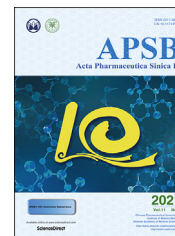




Chinese Pharmaceutical Association
Institute of Materia Medica, Chinese Academy of Medical Sciences

Acta Pharmaceutica Sinica B

www.elsevier.com/locate/apsb
www.sciencedirect.com



ORIGINAL ARTICLE

Homo-PROTAC mediated suicide of MDM2 to treat non-small cell lung cancer



Shipeng He^{b,†}, Junhui Ma^{a,†}, Yuxin Fang^a, Ying Liu^b, Shanchao Wu^a,
Guoqiang Dong^{a,*}, Wei Wang^{c,*}, Chunquan Sheng^{a,d,*}

^aSchool of Pharmacy, Second Military Medical University, Shanghai 200433, China

^bInstitute of Translational Medicine, Shanghai University, Shanghai 200444, China

^cDepartment of Pharmacology and Toxicology and BIO5 Institute, University of Arizona, Tucson, AZ 85721, USA

^dSchool of Medicine, Tongji University, Shanghai 200072, China

Received 5 August 2020; received in revised form 6 November 2020; accepted 17 November 2020

KEY WORDS

Homo-PROTAC;
MDM2;
Self-degradation;
In vivo antitumor activity

Abstract The dose-related adverse effects of MDM2–P53 inhibitors have caused significant concern in the development of clinical safe anticancer agents. Herein we report an unprecedented homo-PROTAC strategy for more effective disruption of MDM2–P53 interaction. The design concept is inspired by the capacity of sub-stoichiometric catalytic PROTACs enabling to degrade an unwanted protein and the dual functions of MDM2 as an E3 ubiquitin ligase and a binding protein with tumor suppressor P53. The new homo-PROTACs are designed to induce self-degradation of MDM2. The results of the investigation have shown that PROTAC **11a** efficiently dimerizes MDM2 with highly competitive binding activity and induces proteasome-dependent self-degradation of MDM2 in A549 non-small cell lung cancer cells. Furthermore, markedly, enantiomer **11a-1** exhibits potent *in vivo* antitumor activity in A549 xenograft nude mouse model, which is the first example of homo-PROTAC with *in vivo* therapeutic potency. This study demonstrates the potential of the homo-PROTAC as an alternative chemical tool for tumorigenic MDM2 knockdown, which could be developed into a safe therapy for cancer treatment.

© 2021 Chinese Pharmaceutical Association and Institute of Materia Medica, Chinese Academy of Medical Sciences. Production and hosting by Elsevier B.V. This is an open access article under the CC BY-NC-ND license (<http://creativecommons.org/licenses/by-nc-nd/4.0/>).

*Corresponding authors. Tel./fax: +86 21 81871239.

E-mail addresses: dgq-81@163.com (Guoqiang Dong), wwang@pharmacy.arizona.edu (Wei Wang), shengcq@hotmail.com (Chunquan Sheng).

[†]These authors made equal contributions to this work.

Peer review under responsibility of Chinese Pharmaceutical Association and Institute of Materia Medica, Chinese Academy of Medical Sciences.

<https://doi.org/10.1016/j.apsb.2020.11.022>

2211-3835 © 2021 Chinese Pharmaceutical Association and Institute of Materia Medica, Chinese Academy of Medical Sciences. Production and hosting by Elsevier B.V. This is an open access article under the CC BY-NC-ND license (<http://creativecommons.org/licenses/by-nc-nd/4.0/>).

1. Introduction

P53 is a crucial tumor suppressor that promotes the apoptosis of cancer cells and prevents tumor development. Moreover, P53 possesses the function of gene repair, which plays a protective role in human healthy¹. Notably, nearly 50% of human cancers are associated with abnormal P53 activity². The interaction between P53 and human murine double minute-2 (MDM2) is the main factor leading to the inactivation of the normal biological function of P53. MDM2 is one of the pivotal suppressors of P53, and overexpressed MDM2 can downregulate the expression of P53 through a negative feedback pathway^{3–5}. Inhibition or degradation of MDM2 protein blocks MDM2–P53 interaction, upregulates the expression of P53 and thus exerts antitumor activity^{6–8}. The development of antitumor agents targeting the MDM2–P53 interaction has become a promising strategy for cancer therapy. Several small-molecule inhibitors of MDM2–P53 have entered into the clinical trial stages^{9,10}. However, many years of efforts have not yielded a single clinically approved agent. One of the main reasons arises from various dose-related adverse effects of MDM2–P53 inhibitors have been observed during clinical studies, particularly the risk to cause hematological diseases^{11,12}. Overcoming this challenging issue may open a new avenue but requires a new paradigm for the design of conceptually distinct regulators to more safely mediate the MDM2–P53 interaction.

Emerging proteolysis targeting chimeras (PROTACs) offer new opportunities for exploiting undruggable or ineffective drug targets *via* the degradation of undesired proteins^{13–19}. Generally, a PROTAC is a heterobifunctional molecule with the capacity to specifically bind to both a target protein of interest and an E3 ubiquitin ligase, and induce rapid protein degradation without the necessity of modification of the target protein^{20–22}. Notably, several small-molecule PROTACs have entered the clinical trial stages to treat multiple cancer types^{23–26}. The unrivalled feature of this technology is a sustained cellular effect to degrade the target protein with only the addition of sub-stoichiometric amount of PROTACs. Therefore, the degradation concentration is orders of magnitude lower than the inhibitory concentration of its constitutive counterpart, and because only a very low dose is required, fewer side effects may result.

Blocking the MDM2–P53 interaction by the targeted degradation strategy is expected to achieve improved efficacy and sustained pharmacological effect^{13,15,27}. Until now, the widely used heterobifunctional PROTACs have been designed targeting the MDM2–P53 interaction²⁸. However, the heterobifunctional PROTAC is a double-edged sword. In addition to exerting the recruitment of the target protein, the heterobifunctional PROTAC also introduces the second target, E3 ubiquitin ligase²⁹. When binding to the E3 ubiquitin ligase, it may result in the inhibition of other proteins and thus generate adverse effects. For example, recent studies have shown that CRBN-based PROTACs degrade both the target protein and other proteins, causing off-target effects in the meantime^{30–32}. Therefore, it is highly desirable to design a PROTAC that specifically degrades MDM2 protein without introducing other targets and decreases the potential side effects.

Overexpression of E3 ubiquitin ligases, such as MDM2, is generally observed in human cancer cells and is associated with poor clinical prognosis or drug resistance¹². Due to the lack of enzymatic activity of E3 ubiquitin proteins, the inhibition of E3 ligase function is usually achieved by targeting protein–protein interactions. It is difficult to develop small-molecule inhibitors

that can effectively decrease the efficacy of E3 ubiquitin ligases^{33,34}. We envision that designing tailored homo-PROTACs that recruit two identical molecules of the same E3 ligase (*e.g.*, MDM2) could trigger its self-degradation by the ubiquitin–proteasome system³⁵. Although conceptual VHL- and CRBN-based homo-PROTACs have been reported for effective self-degradation of E3 ubiquitin ligase^{35–37}, the therapeutic application of the strategy remains unknown, and *in vivo* therapeutic potency has not been attained for any of them.

Considering the dual functions of MDM2 as an antitumor target and an E3 ubiquitin ligase, a homo-PROTAC targeting MDM2 may lead to a distinct, effective strategy in cancer therapy. Inspired by our previous efforts to design small molecules targeting MDM2–P53 interaction^{38–41}, herein the first homo-PROTACs targeting MDM2 have been successfully developed. They exhibit excellent MDM2 binding activity and induce proteasome-dependent self-degradation of MDM2 in non-small cell lung cancer cells. Furthermore, PROTAC **11a-1** exhibits potent *in vivo* antitumor activity in a xenograft mouse model using A549 human lung adenocarcinoma cells, which is the first example of a homo-PROTAC possessing *in vivo* therapeutic potency.

2. Results and discussion

2.1. Rational design of nutlin-based homo-PROTACs

cis-Biphenyl-substituted imidazoline compound **2** is a derivative of Nutlin-3 (**1**, a classic MDM2 inhibitor), which effectively inhibits MDM2 protein and up-regulated P53 protein by negative feedback regulation^{30,42}. MDM2 also belongs to a class of E3 ubiquitin ligase. We proposed to design a homo-PROTAC by connecting two MDM2 ligands through appropriate linkers. Herein compound **2** was selected as the MDM2 binding moiety for homo-PROTAC design. Analysis of the docking model of compound **2** with MDM2 revealed that the piperazine-containing N3 side chain on compound **2** was directly exposed to the solvent and may represent a suitable position for introducing a linker and another MDM2 ligand to obtain a homo-PROTAC (Fig. 1B). Also, various linkers bridging the N3 position of two molecules of compound **2** were investigated to probe the degradation efficiency (Supporting Information for chemical synthesis). It is expected that when the homo-PROTAC simultaneously binds to MDM2 (E3 ubiquitin ligase), MDM2 will be degraded by proteasome in a “suicide” cleavage manner (Fig. 1C).

2.2. Chemistry

The procedure for the synthesis of the key intermediates **5** and **7** is outlined in Scheme 1. Commercially available 1-Boc-piperatine and compound **3** were condensed *via* nucleophilic substitution reaction to obtain intermediate **4**. After deprotection, key intermediate **5** was obtained. Intermediate **3** and 1-Boc-piperatine were reacted in the existence of lewis base to obtain compound **6**, which was subsequently subjected to ester hydrolysis reaction to give corresponding carboxylic acids **7**.

Reaction between intermediates **5** and **8** in the presence of K₂CO₃ in MeCN at 80 °C gave compound **9**. Then, target compounds **10a–f** were afforded by reacting intermediate **5** with commercially available compounds **12a–f** in the condition of HBTU in DMF at room temperature (Scheme 2).

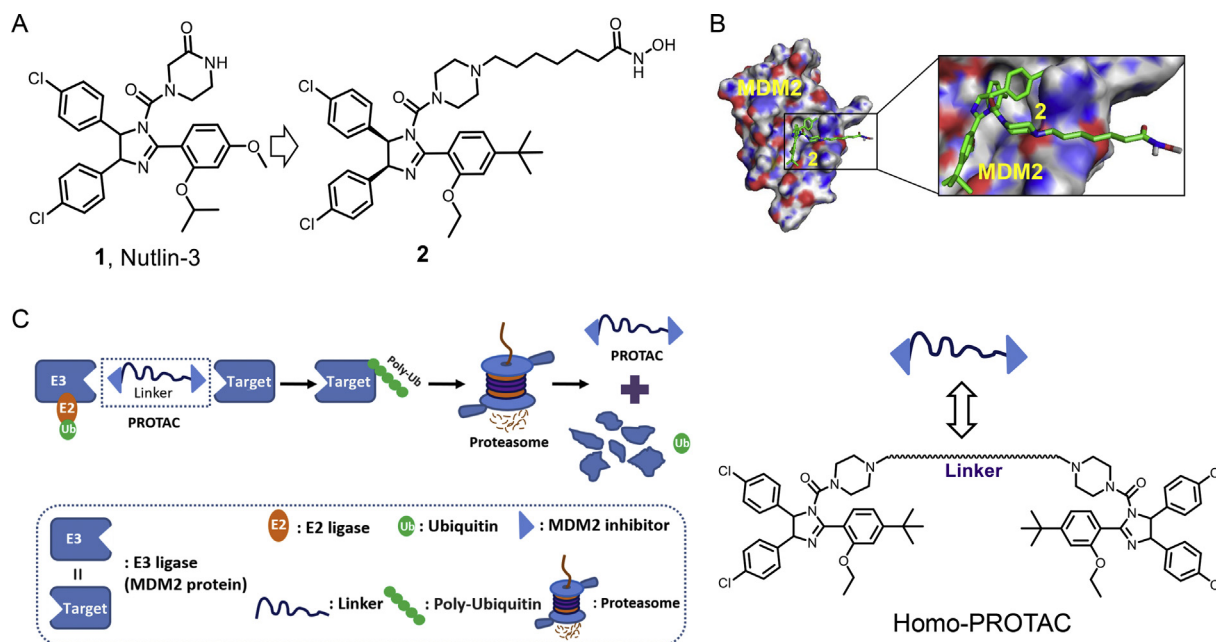


Figure 1 Homo-PROTAC design strategy. (A) Chemical structures of compounds **1** and **2**; (B) The binding model of compound **2** with MDM2 (PDB: 4IPF); (C) Illustration of homo-PROTAC-induced protein ubiquitination and degradation.

Finally, condensation reaction between compound **7** and commercially available reagents **13a–c** yielded title compounds **11a–c** (Scheme 3).

2.3. Study of structure–activity relationships

It was reported that the degradation efficiency of a PROTAC depended on its affinity to bind with the target protein^{28,43}. To investigate the binding affinity of homo-PROTACs, MDM2–P53 competitive binding activities were tested through a fluorescence polarization (FP) binding assay⁴¹ (Table 1 and Fig. 2A), and compound **1** was used as the positive control. Initially, compounds **9** and **10a–d** containing alkyl linkers of different lengths were analyzed. With the increasing length of the alkyl linker, the MDM2–P53 competitive binding affinity was correspondingly decreased, demonstrating that the long alkyl linker might not be favorable for MDM2 binding. For example, compounds **10c** and **10d**, which possess a long linker, were almost inactive ($K_i = 26$ and $39 \mu\text{mol/L}$, respectively). In contrast, compound **10a** with a short linker showed the greatest MDM2–P53 competitive binding activity ($K_i = 0.65 \mu\text{mol/L}$). Exchanging the alkyl linker for a polyethylene glycol (PEG) type chain resulted in enhanced MDM2–P53 competitive binding activities (K_i of **10e** = $1.5 \mu\text{mol/L}$, K_i of **10f** = $0.22 \mu\text{mol/L}$). When the linker length of **10f** was extended by adding a flexible imino group, PROTAC **11a** exhibited increased MDM2–P53 competitive binding activity ($K_i = 0.1 \mu\text{mol/L}$) that was almost 1.5-fold more potent than that of positive control **1**. Unlike the alkyl linker, decreasing the linker length of **11a** resulted in a significant decrease in MDM2–P53 competitive binding activity (K_i of **11b** = $1.8 \mu\text{mol/L}$, K_i of **11c** = $12 \mu\text{mol/L}$).

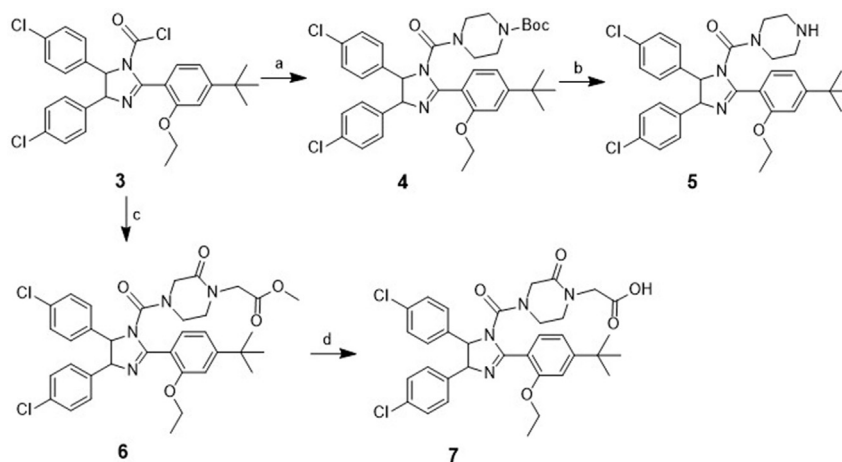
2.4. Antitumor activities *in vitro*

We further evaluated the antiproliferative activities of all homo-PROTACs against four human cancer cell lines, A549 (lung

cancer) cells, HepG2 (liver cancer) cells, HCT116 (colon cancer) cells, and MCF-7 (breast cancer) cells, by the CCK-8 (Cell Counting Kit-8) assay⁴⁴. As shown in Table 1, the *in vitro* anti-proliferation efficacies were generally consistent with the MDM2–P53 competitive binding activities. For example, compounds **10a–b** and **10e–f** with higher MDM2–P53 competitive binding affinity exhibited more potent than that of compounds **9**, **10c–d**, and **11c**. Moreover, compounds with interoxxygenated chains exhibited increased *in vitro* antitumor activity as compared to those containing fat chains. For example, compounds containing an alkyl linker (**9** and **10b–d**) exhibited poor *in vitro* anti-proliferative activities. The loss of antitumor activities was observed when the alkyl linker chain exceeded a certain length (e.g., compounds **10c–d**). Compounds **10a**, **10f**, and **11a** exhibited satisfactory antiproliferative activity with a broad spectrum, and were more potent than that of the positive control. Particularly, compound **11a**, the most potent MDM2 binder, exhibited the highest antiproliferative activity against A549 cancer cells ($\text{IC}_{50} = 1.0 \mu\text{mol/L}$).

2.5. Effects of target compounds on MDM2 degradation

In consideration of molecular and cellular activities, compounds **10a**, **10f**, and **11a** were chosen for further evaluation of the effects on MDM2 degradation and P53 expression in A549 cell line by analysis of Western blotting, and compound **1** was used as positive control (Fig. 2B). The results showed that compounds **10f** and **11a** dose-dependently induced MDM2 protein cleavage and increased the P53 protein expression in A549 cells. Particularly, compound **11a** exhibited a higher potency for MDM2 degradation than that of compound **10f** at the same concentrations. Compound **11a** achieved degradation concentration DC_{50} (concentration causing 50% protein degradation) values of $1.01 \mu\text{mol/L}$ and induced >95% MDM2 degradation at a concentration of $2 \mu\text{mol/L}$ in A549 cells for 24 h (Fig. 2E). However, no degradation was observed in A549 cells when they were treated with compound



Scheme 1 Reagents and conditions: (a) 1-Boc-piperazine (1.1 eq.), Et₃N (2.0 eq.), DCM, rt, 1.0 h, yield 91%; (b) CF₃COOH (6.0 eq.), DCM, rt, 2.0 h, yield 95%; (c) methyl 2-(2-oxopiperazin-1-yl) acetate (1.2 eq.), Et₃N (1.0 eq.), DCM, rt, 2.0 h, yield 82%; (d) LiOH (2.3 eq.), THF:MeOH:H₂O = 3:2:1, rt, 1.5 h, yield 90%.

10a. In addition, the cellular permeability assay was performed to assess the cellular permeability. The results showed that compound **11a** had low permeability, which might be the reason for the moderate degradation efficiency in A549 cells (Supporting Information Table S1). Control assays clearly indicated that compound **1** at equimolar concentrations did not induce the degradation of MDM2 in A549 cells. Moreover, additional compounds (**9**, **10b–e**, and **11b–c**) were further assayed, although they failed to induce the degradation of MDM2 in A549 cells at 2.5 μmol/L for 24 h (Fig. 2F).

2.6. Mechanism used by compound **11a** to degrade MDM2

To explore whether the degradation of MDM2 is dependent on the proteasome and results in the death of A549 cells, we used MG132⁴⁵, an inhibitor of the proteasome, to pre-treat A549 cells at 0.1 or 0.2 μmol/L for 8 h. Then, compound **11a** was added to the pre-treated A549 cells for another 48 h. We predicted that MG132 would be able to effectively reduce growth inhibitory activity of **11a** on A549 cells, but it would have no effect on the activity of compound **1**. Indeed, pre-treatment with MG132 in a concentration-dependent manner reduced the inhibitory activity of **11a** on A549 cells to the same level as that of compound **1** (Fig. 3A). These results verified that MDM2 degradation mediated by compound **11a** was dependent on the proteasome, which further induced the death of A549 cells.

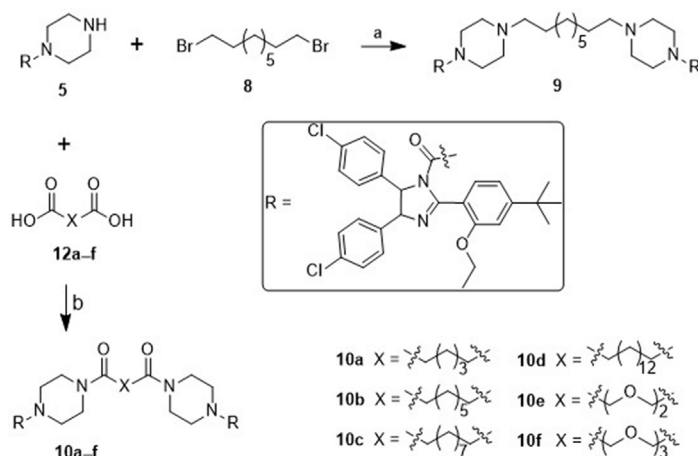
Given that MDM2 degradation is a well-known marker for A549 cells apoptosis⁴⁶, we performed flow cytometric analysis to evaluate the antitumor mechanism of compound **11a** (Fig. 3B and C). Treatment with MG132 showed no toxic effect on the A549 cells at 0.2 μmol/L after incubation for 24 h. It was found that compound **11a** induced 23.49% apoptosis in A549 cells at 5.0 μmol/L after 24 h treatment, whereas only 15.81% apoptosis were detected upon treatment with compound **11a** and MG132 in combination. In addition, compound **1** and MG132 in combination (12.64% apoptosis) failed to decrease the A549 cell apoptosis compare to that of compound **1** alone (10.94% apoptosis) under the same conditions. The result suggested that compound **11a** induced A549 cells apoptosis by the ubiquitin–proteasome system.

2.7. Biochemical evaluations of enantiomers of compound **11a**

The enantiomers of compound **11a** were isolated by chiral chromatography, and their values of optical rotation were determined through a polarimeter. In addition, three configurations of compound **11a** enantiomers were identified by comparing the optical rotation values with those of compound **1** enantiomers (Supporting Information Fig. S1). The FP binding assay indicated that the enantiomers had different MDM2–P53 competitive binding activities (Fig. 4A). The mesomer **11a-2** had a K_i value of 0.12 μmol/L. Interestingly, enantiomer **11a-1** ($K_i = 0.09$ μmol/L, Table 2) exhibited an effectiveness that was almost 110-fold greater than that of enantiomer **11a-3** ($K_i = 9.9$ μmol/L), and was superior to compound **1** ($K_i = 0.15$ μmol/L).

Furthermore, CCK-8 assay was used to investigate the effect of enantiomers **11a** on cell viability in the A549 and HCT116 cell line. Similar to MDM2–P53 inhibitor **1**, PROTAC **11a** exerted its antitumor activity by influencing the expression of P53 because enantiomers of **11a** had better inhibitory activity against P53-wild HCT116 cells than the P53-deleted HCT116 cells (Table 2). In addition, consistent with the MDM2 competitive binding activity, enantiomer **11a-1** also exhibited the best antiproliferative activity among the three enantiomers. Particularly, enantiomer **11a-1** exhibited the best inhibitory activity with the IC₅₀ value of 0.58 μmol/L for the A549 cells, which was more effective than that of racemate **11a** (IC₅₀ = 1.4 μmol/L) and reference compound **1** (IC₅₀ = 9.9 μmol/L).

Next, the ability of **11a** enantiomers for MDM2 degradation was evaluated by Western blotting analysis. Enantiomer **11a-1** dose-dependently induced the degradation of MDM2 and up-regulated the expression of P53 through the negative feedback loop in A549 cells after 24 h whereas the enantiomer **11a-3** and mesomer **11a-2** could not induce the cleavage of MDM2 under the same conditions (Fig. 4C). These results demonstrated that the chiral center on the imidazole scaffold of compound **11a** is important to MDM2 binding and degradation, and enantiomer **11a-1** was the preferential conformation of compound **11a**. Next, the time course degradation experiment was performed to assess the kinetics of MDM2 degradation caused by **11a** and **11a-1**. As shown in Fig. 4D, compounds **11a** and **11a-1** induced MDM2 degradation in a time-dependent manner and the depletion of



Scheme 2 Reagents and conditions: (a) K_2CO_3 (2.5 eq.), MeCN, 80 °C, 5.0 h, yield 57%; (b) HBTU (3.8 eq.), DIPEA (3.8 eq.), DMF, rt, 1.0–2.0 h, yield 72%–85%.

MDM2 was observed as early as 2 h after treatment. In order to further explore whether the degradation of MDM2 is based on proteasome pathway, the proteasome inhibitor MG132 was used to rescue the MDM2 degradation. As depicted in Fig. 4F, MG132 blocked the MDM2 degradation induced by **11a** and **11a-1** in A549 cells. Finally, the mRNA level of *MDM2* didn't exhibit obvious change after treatment with **11a-1** in A549 cells (Fig. 4E), which demonstrated that compound **11a-1** could not affect the *MDM2* mRNA level and acted as a bona fide MDM2 degrader.

2.8. *In vivo* antitumor activity of compound **11a-1**

A bottleneck in current PROTAC-based drug discovery has been created by the limited *in vivo* efficacy due to large molecular weights and unfavorable physicochemical properties. Thus, the *in vivo* antitumor activity of enantiomer **11a-1** was evaluated by the A549 xenograft model. The results demonstrated that compound **11a-1** effectively inhibited the A549 tumor growth in a concentration-dependent manner compared with vehicle control (Fig. 5A). Intraperitoneal injection of compound **11a-1** at a dose of 20 mg/kg twice-daily for 21 continuous days achieved tumor growth inhibition (TGI) of 45.6%, which was comparable to MDM2 inhibitor **1** under the same dose (TGI = 47.8%). When the dosage was increased to 30 mg/kg, treatment with compound **11a-1** achieved a TGI of 52.4%. Importantly, compound **11a-1** at both doses was well tolerated and caused minimal weight loss in mice (Fig. 5B). Thus, PROTAC **11a-1** showed potent *in vivo* efficacy in the induction of tumor regression at well-tolerated doses. Western blotting assay was used to detect the expression of P53 and MDM2 in tumor tissues. As shown in Fig. 5C, compound **11a-1** dose-dependently increased the expression of P53, which was more effective than that of compound **1**. In contrast, the expression level of MDM2 was decreased, indicating the efficient degradation of MDM2 induced by **11a-1** in mice. In addition, pharmacokinetic (PK) profiles of compound **11a-1** were evaluated in Sprague–Dawley (SD) rats administered intravenously (i.v.) at 2 mg/kg (Fig. 5D and E). The terminal half-life and area under the curve (AUC) of compound **11a-1** was approximately 9.6 h and 42,835 h·ng/mL, respectively. The PK data indicated that compound **11a-1** could achieved good plasma exposure in rats.

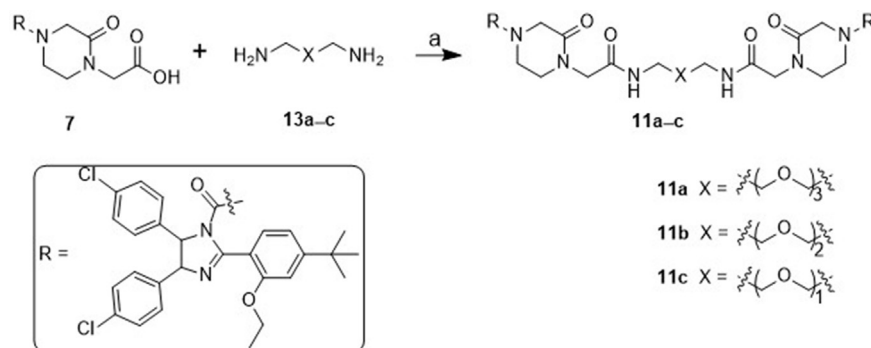
3. Conclusions

In summary, a series of novel homo-PROTACs have been designed and evaluated for self-degradation of MDM2. The biological assays uncovered that compound **11a** possesses potent activities both in molecular and cellular level. Antitumor mechanism studies revealed that compound **11a** induced MDM2 degradation and increased P53 expression in a dose-dependent manner. It significantly induced the apoptosis of A549 cell line *via* a ubiquitin–proteasome pathway. In particular, enantiomer **11a-1** exhibited potent *in vivo* antitumor activity in A549 xenograft model (TGI = 52%). Taken together, this study highlights the effectiveness of MDM2-based homo-PROTACs as a new cancer treatment strategy. PROTAC **11a** represents a promising lead compound that can be used for further optimization and biological studies. The homo-PROTAC approach may offer an opportunity to overcome the challenge of the dose-related adverse effects of MDM2–P53 inhibitors that remains as an obstacle to be overcome in the field of clinical anticancer agent development.

4. Experimental

4.1. Chemistry

All reagents and solvents were obtained commercially and used without further purification. 1H NMR and ^{13}C NMR spectra were collected by Bruker AVANCE300 or AVANCE600 spectrometers (Leipzig, Bruker Company, Germany), using tetramethylsilane (TMS) as an interior label and dimethyl sulfoxide (DMSO)- d_6 as solvents. Chemical shifts (δ) are expressed in parts per million (ppm). The mass spectra (MS) were measured on an Esquire 3000 LC–MS mass spectrometer. The analysis of thin-layer chromatography (TLC) was performed with GF254 silica gel plates to detect reactions (Haiyang Chemical, Qingdao, China), and visualization of reactants occurred under 254 nm UV light. Silica gel column chromatography was carried out with Silica Gel 60 G (Haiyang Chemical). High-performance liquid chromatography (HPLC) analyses were performed on an Agilent Technologies 1206, instrument to determine purity, and water and methanol were used as the mobile phase.



Scheme 3 Reagents and conditions: (a) HBTU (3.8 eq.), DIPEA (3.8 eq.), DMF, rt, 1.0–2.0 h, yield 61%–85%.

Table 1 MDM2–P53 competitive binding and *in vitro* antitumor activities of designed homo-PROTAC.

Compd.	Linker	MDM2–P53 K_i ($\mu\text{mol/L}$)	IC ₅₀ ($\mu\text{mol/L}$)			
			A549	HepG2	HCT116	MCF-7
9		10 ± 0.62	11 ± 2.0	11 ± 3.4	9.7 ± 1.4	11 ± 1.1
10a		0.65 ± 0.17	2.1 ± 0.1	1.5 ± 0.05	2.5 ± 1.0	2.1 ± 0.0
10b		1.6 ± 0.96	6.3 ± 1.2	3.8 ± 0.0	5.7 ± 1.3	6.3 ± 1.1
10c		26 ± 7.9	>50	>50	>50	>50
10d		39 ± 8.6	>50	>50	>50	>50
10e		1.5 ± 0.82	6.6 ± 1.0	4.6 ± 0.8	3.9 ± 0.7	7.4 ± 0.51
10f		0.22 ± 0.07	1.3 ± 0.0	1.2 ± 0.2	1.3 ± 0.1	4.7 ± 0.81
11a		0.10 ± 0.02	1.0 ± 0.1	3.3 ± 0.31	1.9 ± 0.11	2.9 ± 0.6
11b		1.8 ± 0.94	6.6 ± 1.0	7.3 ± 0.52	3.9 ± 1.6	4.9 ± 0.2
11c		12 ± 1.9	9.3 ± 1.7	12 ± 3.7	7.4 ± 2.1	14 ± 3.7
1		0.15 ± 0.02	7.9 ± 1.3	8.9 ± 1.0	5.0 ± 0.9	9.7 ± 1.0

Values were represented as mean ± standard deviation (SD) of at least two independent assays.

4.1.1. Nonane-1,9-diylbis(piperazine-4,1-diyl)bis((2-(4-(*tert*-butyl)-2-ethoxyphenyl)-*cis*-4,5-bis(4-chlorophenyl)-4,5-dihydro-1*H*-imidazole-1-yl) methanone (**9**)

To a solution of compound **5** (200 mg, 0.35 mmol) in 10 mL MeCN, 1,9-dibromononane (50 mg, 0.18 mmol) and K₂CO₃ (120 mg, 0.86 mmol) were slowly added. After the reaction, the mixture was stirred at 80 °C for 5 h. Then the resulting solution was cooled to room temperature and the organic solvent was removed under the reduced pressure distillation to obtain the impure product which was further purified by column chromatography (CH₂Cl₂:MeOH = 100:2) to obtain compound **9** (128 mg, 57%) as off-white solid. ¹H NMR (DMSO-*d*₆, 150 MHz) δ : 1.18–1.30 (m, 14H), 1.29 (t, J = 6.93 Hz, 6H), 1.32 (s, 18H), 1.63–1.76 (m, 8H), 1.99 (t, J = 7.05 Hz, 4H), 2.85–3.06 (m, 8H), 4.02–4.20 (m, 4H), 5.50 (d, J = 9.92 Hz, 2H), 5.65 (d,

J = 9.92 Hz, 2H), 6.94 (d, J = 7.59 Hz, 4H), 6.99 (d, J = 8.76 Hz, 4H), 7.05 (s, 2H), 7.08 (t, J = 7.89 Hz, 6H), 7.13 (t, J = 8.76 Hz, 4H), 7.48 (d, J = 7.95 Hz, 2H). ¹³C NMR (DMSO-*d*₆, 150 MHz) δ : 14.9, 26.6, 27.1, 28.6, 29.1, 31.5, 32.4, 35.4, 45.8, 51.8, 64.0, 68.4, 71.0, 109.2, 117.5, 117.9, 127.9, 129.1, 130.1, 130.7, 131.5, 137.0, 137.9, 155.5, 157.0, 160.3. HRMS m/z Calcd. for C₇₃H₈₉Cl₄N₈O₄ [M+H]⁺ 1283.5726, Found 1283.5719. HPLC purity: 95.7%.

4.1.2. 1,7-Bis(4-(2-(4-(*tert*-butyl)-2-ethoxyphenyl)-*cis*-4,5-bis(4-chlorophenyl)-4,5-dihydro-1*H*-imidazole-1-carbonyl) piperazine-1-yl) heptane-1,7-dione (**10a**)

To a solution of heptanedioic acid (29 mg, 0.18 mmol) in 10 mL anhydrous DMF, HBTU (266 mg, 0.72 mmol), DIPEA (0.14 mL, 0.72 mmol) and **5** (202 mg, 0.35 mmol) were added. The mixture

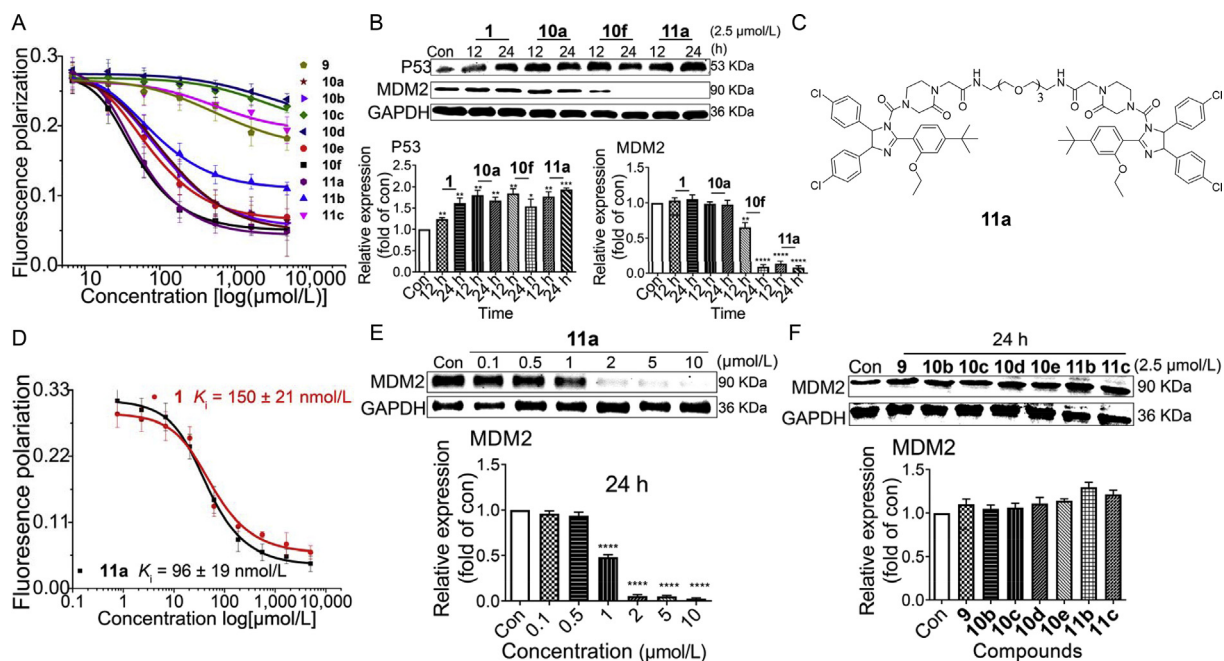


Figure 2 Degradation activity of compound **11a**. (A) The curves of MDM2 competitive binding activities of all target compounds. (B) Effects of treated compounds **10a**, **10f**, and **11a** on P53 and MDM2 protein in A549 cells via the analysis of Western blotting for 12 and 24 h at 2.5 $\mu\text{mol/L}$. (C) The structure of compound **11a**. (D) The curves of MDM2–P53 competitive binding activities of compounds **11a** and **1**. (E) Compound **11a** induced degradation of MDM2 in the A549 cell line after treatment for 24 h at gradient concentrations. (F) Additional compounds induced degradation of MDM2 in the A549 cell line after treatment for 24 h at 2.5 $\mu\text{mol/L}$. Western blotting were analyzed and quantitated using the ImageQuant program. The data are represent as the mean \pm SD, $n = 3$. * $P < 0.05$, ** $P < 0.01$, *** $P < 0.005$, and **** $P < 0.001$ vs. vehicle control. Con: control.

reaction was stirred at room temperature for 1.5 h. Then the reaction mixture was dissolved in EtOAc (10 mL) and washed successively with water (10 mL) and saturated NaCl solution (10 mL), the organic phase was dried with anhydrous Na_2SO_4 . After filtration, the filtrate was further purified by column chromatography (CH_2Cl_2 :MeOH = 100:2) to afford compound **10a** (190 mg, 85% yield) as off-white solid. ^1H NMR (DMSO- d_6 , 600 MHz) δ : 1.12–1.16 (m, 4H), 1.26 (s, 18H), 1.28 (t, $J = 6.97$ Hz, 6H), 1.30 (m, $J = 5.09$ Hz, 2H), 2.11 (t, $J = 7.41$ Hz, 4H), 2.67–2.85 (m, 8H), 2.86–3.00 (m, 8H), 4.06 (t, $J = 13.37$ Hz, 7.21 Hz, 4H), 5.51 (d, $J = 9.26$ Hz, 2H), 5.65 (d, $J = 9.26$ Hz, 2H), 6.93 (d, $J = 8.06$ Hz, 4H), 6.98 (d, $J = 8.34$ Hz, 4H), 7.04 (s, 2H), 7.05–7.09 (m, 6H), 7.14 (d, $J = 8.13$ Hz, 4H), 7.52 (d, $J = 7.85$ Hz, 2H); ^{13}C NMR (DMSO- d_6 , 150 MHz) δ : 14.9, 24.9, 28.9, 31.4, 32.6, 35.4, 44.3, 45.9, 46.3, 64.1, 68.3, 71.0, 109.2, 117.4, 117.9, 127.9, 129.1, 130.2, 130.9, 131.5, 131.6, 136.9, 137.8, 155.7, 155.9, 157.1, 160.2, 171.1. HRMS m/z Calcd. for $\text{C}_{71}\text{H}_{81}\text{Cl}_4\text{N}_8\text{O}_6$ $[\text{M}+\text{H}]^+$ 1281.5028, Found 1281.5044. HPLC purity: 96.4%.

The synthesis procedure of target compounds **10b–d** were similar to that of compound **10a**.

4.1.3. 1,9-Bis(4-(2-(4-(tert-butyl)-2-ethoxyphenyl)-cis-4,5-bis(4-chlorophenyl)-4,5-dihydro-1H-imidazole-1-carbonyl)piperazin-1-yl) nonane-1,9-dione (**10b**)

^1H NMR (DMSO- d_6 , 600 MHz) δ : 0.80–1.01 (m, 8H), 1.03–1.15 (m, 4H), 1.20–1.32 (m, 4H), 1.34 (t, $J = 10.30$ Hz, 6H), 1.37 (s, 18H), 1.81 (t, $J = 7.10$ Hz, 4H), 2.01 (s, 2H), 2.70–2.83 (m, 2H), 2.85–2.96 (m, 2H), 4.10 (t, $J = 8.00$ Hz, 2H), 4.22 (t, $J = 8.00$ Hz, 2H), 5.80 (s, 2H), 5.90 (s, 2H), 7.05–7.10 (m, 8H), 7.13 (d, $J = 6.58$ Hz, 4H), 7.18 (d, $J = 7.60$ Hz, 8H), 7.50 (s,

2H), 8.62 (s, 2H), 10.33 (s, 2H). ^{13}C NMR (DMSO- d_6 , 150 MHz) δ : 15.1, 21.1, 25.3, 26.1, 29.1, 31.2, 31.5, 32.6, 35.3, 60.3, 64.3, 66.5, 109.4, 117.2, 120.2, 127.9, 129.1, 129.7, 129.9, 130.2, 130.5, 136.5, 137.7, 151.2, 153.3, 156.8, 158.8, 169.5. HRMS m/z Calcd. for $\text{C}_{73}\text{H}_{85}\text{Cl}_4\text{N}_8\text{O}_6$ $[\text{M}+\text{H}]^+$ 1309.5341, Found 1309.5326. HPLC purity: 95.5%.

4.1.4. Nonane-1,9-diylbis(piperazine-4,1-diyl) bis((2-(4-(tert-butyl)-2-ethoxyphenyl)-cis-4,5-bis(4-chlorophenyl)-4,5-dihydro-1H-imidazole-1-yl) methanone (**10c**)

^1H NMR (DMSO- d_6 , 600 MHz) δ : 1.15–1.22 (m, 10H), 1.29 (s, 18H), 1.32 (t, $J = 6.93$ Hz, 6H), 1.33–1.40 (m, 2H), 2.15 (t, $J = 7.43$ Hz, 6H), 2.68–2.85 (m, 8H), 2.86–3.05 (m, 8H), 4.09 (dd, $J = 13.63$ Hz, 6.71 Hz, 4H), 5.54 (d, $J = 9.90$ Hz, 2H), 5.68 (d, $J = 9.90$ Hz, 2H), 6.97 (d, $J = 7.79$ Hz, 4H), 7.03 (d, $J = 8.33$ Hz, 4H), 7.05 (s, 2H), 7.09 (d, $J = 8.32$ Hz, 6H), 7.16 (d, $J = 8.46$ Hz, 4H), 7.55 (d, $J = 7.94$ Hz, 2H). ^{13}C NMR (DMSO- d_6 , 150 MHz) δ : 14.9, 25.1, 29.1, 29.2, 31.3, 32.6, 35.4, 44.3, 45.9, 46.3, 64.1, 68.3, 71.1, 109.2, 117.4, 117.9, 127.9, 129.1, 130.2, 130.9, 131.5, 131.6, 136.9, 137.8, 155.7, 155.9, 157.1, 160.2, 171.1. HRMS m/z Calcd. for $\text{C}_{75}\text{H}_{89}\text{Cl}_4\text{N}_8\text{O}_6$ $[\text{M}+\text{H}]^+$ 1337.5654, Found 1337.5698. HPLC purity: 96.3%.

4.1.5. 1,5-Bis(4-(2-(4-(tert-butyl)-2-ethoxyphenyl)-cis-4,5-bis(4-chlorophenyl)-4,5-dihydro-1H-imidazole-1-carbonyl)piperazin-1-yl) pentane-1,5-dione (**10d**)

^1H NMR (DMSO- d_6 , 600 MHz) δ : 1.19–1.25 (m, 20H), 1.27–1.30 (t, $J = 10.02$ Hz, 6H), 1.29 (s, 18H), 1.34–1.38 (m, 4H), 2.15 (t, $J = 7.32$ Hz, 4H), 2.52–3.01 (m, 16H), 4.01–4.12 (m, 4H), 5.53 (t, $J = 9.76$ Hz, 2H), 5.68 (t, $J = 9.76$ Hz, 2H),

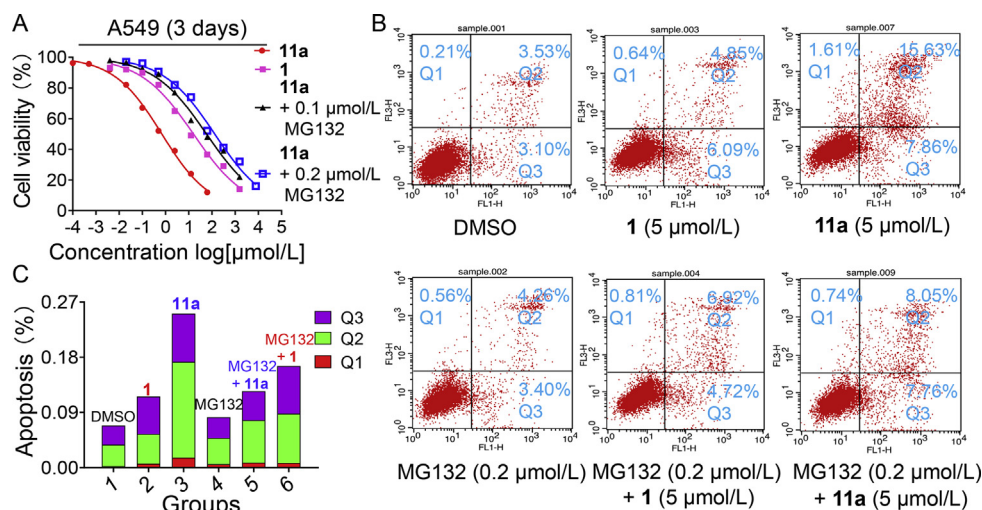


Figure 3 Mechanism of compound **11a** on MDM2 degradation. (A) Effects of compound **11a** on A549 cell viability after pre-treatment with proteasome inhibitor MG132 at different concentrations, using compound **1** as the control group. The data are normalized to the vehicle group. (B) The characterization of apoptosis induced by compound **11a** in the A549 cell line. After two groups of A549 cells were pre-treated with MG132 at 0.2 $\mu\text{mol/L}$ for 8 h, compounds **1** and **11a** were added to the treatment groups for another 48 h. Three groups were each treated with compounds **1**, **11a**, MG132, and vehicle control (DMSO) for 48 h. Apoptosis was tested by a flow cytometry with Annexin V/propidium iodide (PI) double staining. (C) The histogram of apoptosis analysis results.

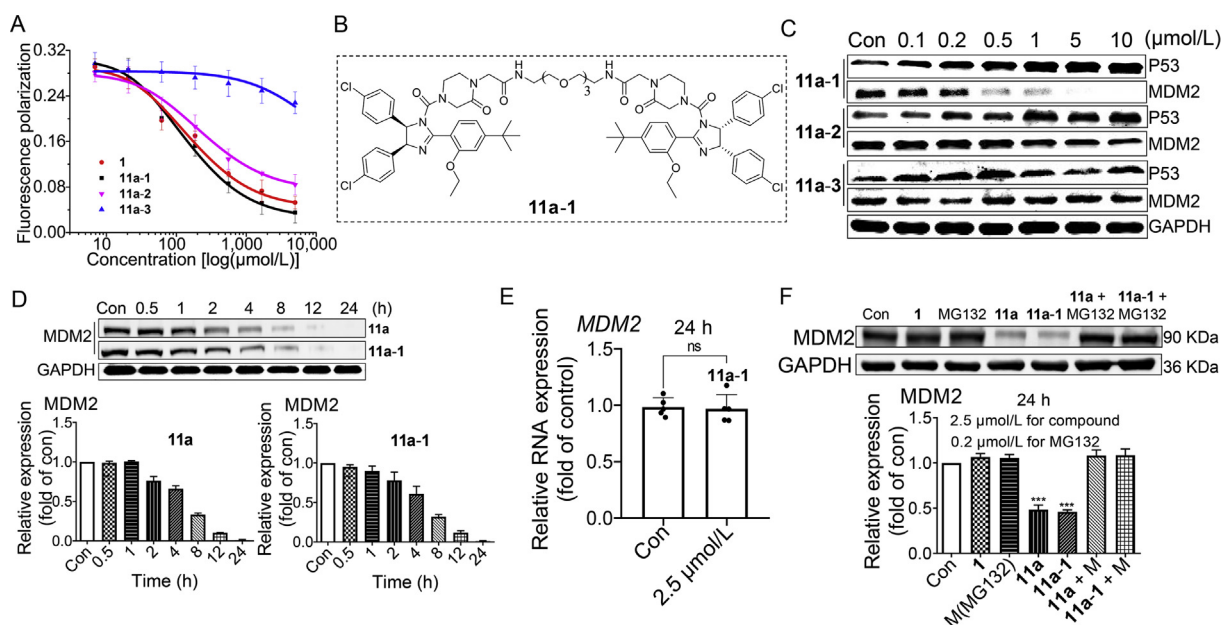


Figure 4 *In vitro* antitumor efficacy of enantiomers of **11a**. (A) The MDM2–P53 competitive binding activities of enantiomers of **11a**. (B) The structure of enantiomer **11a-1**. (C) Analysis of cellular MDM2 and P53 induced by enantiomers of **11a** using Western blotting. Treatment with compounds **11a-1**, **11a-2**, and **11a-3**, induced the degradation of MDM2 after treatment of A549 cells for 24 h at gradient concentrations. (D) The time course degradation of **11a** and **11a-1**. (E) The mRNA level of *MDM2* induced by **11a-1**. (F) The MDM2 degradation rescue experiments by Western blotting. Western blotting were analyzed and quantitated using the ImageQuant program. The data are represent as the mean \pm SD, $n = 3$. * $P < 0.05$, and *** $P < 0.005$ vs. vehicle control. Con: control.

6.96 (t, $J = 7.50$ Hz, 4H), 7.00–7.05 (m, 4H), 7.06 (s, 2H), 7.09 (d, $J = 8.22$ Hz, 6H), 7.16 (d, $J = 8.58$ Hz, 4H), 7.55 (d, $J = 7.95$ Hz, 2H). ^{13}C NMR (DMSO- d_6 , 150 MHz) δ : 14.9, 25.2, 29.1, 29.3, 29.4, 29.5, 31.2, 31.4, 32.6, 35.4, 44.3, 45.4, 45.7, 46.3, 64.1, 68.3, 71.1, 109.2, 117.4, 117.9, 127.9, 129.1, 130.2, 130.9, 131.5, 131.7, 136.9, 137.8, 155.7, 155.9, 157.1, 160.2, 171.1. HRMS m/z Calcd. for $\text{C}_{80}\text{H}_{99}\text{Cl}_4\text{N}_8\text{O}_6$ [M+H] $^+$ 1407.6436, Found 1407.6403. HPLC purity: 95.7%.

4.1.6. 2,2'-(Ethane-1,2-diylbis(oxy)) bis(1-(4-(2-(4-(*tert*-butyl)-2-ethoxyphenyl)-*cis*-4,5-bis(4-chlorophenyl)-4,5-dihydro-1*H*-imidazole-1-carbonyl) piperazin-1-yl) ethan-1-one) (**10e**)

To a solution of 2,2'-(ethane-1,2-diylbis(oxy)) diacetic acid (32 mg, 0.18 mmol) was added HBTU (266 mg, 0.72 mmol), DIPEA (0.14 mL, 0.72 mmol) followed by dropwise addition of **5** (200 mg, 0.35 mmol) in anhydrous DMF (10 mL). After the reaction, the mixture reaction was stirred at room temperature for

Table 2 MDM2–P53 competitive binding and *in vitro* anti-tumor activities of enantiomers **11a**.

Compd.	K_i ($\mu\text{mol/L}$)	IC_{50} ($\mu\text{mol/L}$)		
		A549	HCT116 (P53 ⁺)	HCT116 (P53 ⁻)
11a	0.1 ± 0.2	1.4 ± 0.31	1.9 ± 0.67	>50
11a-1	0.09 ± 0.0	0.58 ± 0.0	1.1 ± 0.31	21 ± 8.3
11a-2	0.12 ± 0.04	8.3 ± 2.2	9.9 ± 1.0	>50
11a-3	9.9 ± 2.3	11 ± 1.4	8.7 ± 2.2	>50
1	0.15 ± 0.02	9.9 ± 1.3	8.6 ± 1.0	19 ± 0.91

Values were expressed as mean ± SD in parallel three times. P53⁺: P53-wild, P53⁻: P53-deleted.

1.5 h. Then the resulting mixture was dissolved in EtOAc (20 mL) and washed successively with water (10 mL) and saturated NaCl solution (10 mL), the organic solvent was dried with anhydrous Na₂SO₄. After filtration, the filtrate was further purified by column chromatography (CH₂Cl₂:MeOH = 100:2) to obtain compound **10e** (182 mg, 81% yield) as off-white solid. ¹H NMR (DMSO-*d*₆, 600 MHz) δ : 1.29 (m, 18H), 1.30 (t, J = 6.97 Hz, 6H), 2.72–2.89 (m, 8H), 2.93–3.05 (m, 8H), 3.44 (s, 4H), 4.01 (s, 4H), 4.09 (dd, J = 13.94 Hz, 7.32 Hz, 4H), 5.55 (d, J = 10.03 Hz, 2H), 5.68 (d, J = 10.03 Hz, 2H), 6.95 (d, J = 8.00 Hz, 4H), 7.03 (d, J = 8.42 Hz, 4H), 7.05–7.15 (m, 8H), 7.17 (d, J = 8.42 Hz, 4H), 7.55 (d, J = 7.90 Hz, 2H). ¹³C NMR (DMSO-*d*₆, 150 MHz) δ : 14.8, 31.4, 35.5, 43.7, 45.9, 46.1, 64.1, 68.3, 69.6, 69.9, 71.1, 109.2, 117.4, 117.9, 127.9, 128.0, 129.2, 130.2, 130.9, 131.6, 131.7, 136.9, 137.8, 155.7, 155.9, 157.1, 160.2, 167.6. HRMS m/z Calcd. for C₇₀H₇₉Cl₄N₈O₈ [M+H]⁺ 1299.4769, Found 1299.4746. HPLC purity: 95.2%.

The synthesis procedure of target compound **10f** was similar to that of compound **10e**.

4.1.7. 2,2'-((Oxybis(ethane-2,1-diyl))bis(oxy))bis(1-(4-(2-(4-(tert-butyl)-2-ethoxyphenyl)-cis-4,5-bis(4-chlorophenyl)-4,5-dihydro-1H-imidazole-1-carbonyl)piperazin-1-yl)ethan-1-one) (**10f**)

¹H NMR (DMSO-*d*₆, 600 MHz) δ : 1.31 (s, 18H), 1.32 (d, J = 7.07 Hz, 6H), 2.71–2.85 (m, 8H), 2.86–2.94 (m, 8H), 3.46 (d, J = 6.23 Hz, 8H), 4.02 (s, 4H), 4.10 (dd, J = 12.87 Hz, 7.06 Hz, 4H), 5.57 (d, J = 9.89 Hz, 2H), 5.69 (d, J = 9.89 Hz, 2H), 6.97 (d, J = 7.64 Hz, 4H), 7.04 (d, J = 8.09 Hz, 4H), 7.05–7.13 (m, 8H), 7.17 (d, J = 7.64 Hz, 4H), 7.56 (d, J = 7.87 Hz, 2H). ¹³C NMR (DMSO-*d*₆, 150 MHz) δ : 14.8, 31.3, 35.4, 43.7, 45.9, 46.1, 64.1, 68.3, 69.7, 69.9, 70.1, 71.0, 109.2, 117.4, 117.8, 127.9, 127.9, 129.2, 130.2, 130.9, 131.1, 131.6, 131.7, 136.8, 137.7, 155.7, 155.9, 157.1, 160.3, 167.7. HRMS m/z Calcd. for C₇₂H₈₃Cl₄N₈O₉ [M+Na]⁺ 1367.4827, Found 1367.4866. HPLC purity: 97.6%.

4.1.8. *N,N'*-(((Oxybis(ethane-2,1-diyl))bis(oxy))bis(ethane-2,1-diyl))bis(2-(4-(2-(4-(tert-butyl)-2-ethoxyphenyl)-cis-4,5-bis(4-chlorophenyl)-4,5-dihydro-1H-imidazole-1-carbonyl)-2-oxopiperazin-1-yl)acetamide) (**11a**)

¹H NMR (DMSO-*d*₆, 600 MHz) δ : 1.29 (t, J = 6.77 Hz, 6H), 1.33 (s, 18H), 2.86 (s, 4H), 3.17 (d, J = 5.45 Hz, 4H), 3.22 (d, J = 5.08 Hz, 2H), 3.37 (d, J = 5.64 Hz, 4H), 3.48 (s, 8H), 3.60 (d, J = 18.05 Hz, 2H), 3.68–3.72 (m, 4H), 3.81 (d, J = 16.17 Hz,

4H), 4.04–4.13 (m, 4H), 5.61 (d, J = 9.83 Hz, 2H), 5.70 (d, J = 9.83 Hz, 2H), 6.98 (d, J = 7.71 Hz, 4H), 7.05 (d, J = 6.21 Hz, 6H), 7.08 (d, J = 7.52 Hz, 2H), 7.14 (dd, J = 7.90 Hz, 25.58 Hz, 8H), 7.55 (d, J = 7.28 Hz, 2H), 7.94 (s, 2H). ¹³C NMR (DMSO-*d*₆, 150 MHz) δ : 14.9, 29.4, 30.3, 31.4, 31.6, 35.4, 39.0, 42.7, 46.8, 49.0, 49.3, 64.1, 68.4, 69.4, 70.0, 71.6, 109.3, 117.6, 127.9, 129.2, 130.1, 130.8, 131.6, 131.7, 136.7, 137.8, 154.8, 155.8, 156.6, 160.4, 164.8, 167.7. HRMS m/z Calcd. for C₇₆H₈₉Cl₄N₁₀O₁₁ [M+H]⁺ 1460.5465, Found 1460.5474. HPLC purity: 95.5%.

4.1.9. *N,N'*-((Ethane-1,2-diylbis(oxy))bis(ethane-2,1-diyl))bis(2-(4-(2-(4-(tert-butyl)-2-ethoxyphenyl)-cis-4,5-bis(4-chlorophenyl)-4,5-dihydro-1H-imidazole-1-carbonyl)-2-oxopiperazin-1-yl)acetamide) (**11b**)

¹H NMR (DMSO-*d*₆, 600 MHz) δ : 1.29 (t, J = 6.76 Hz, 6H), 1.33 (s, 18H), 2.86 (s, 4H), 3.17 (dd, J = 6.76 Hz, 11.44 Hz, 4H), 3.18–3.24 (m, 2H), 3.37 (t, J = 5.86 Hz, 6H), 3.47 (s, 4H), 3.60 (d, J = 17.36 Hz, 2H), 3.68–3.72 (m, 4H), 3.80 (d, J = 16.23 Hz, 2H), 4.03–4.15 (m, 4H), 5.61 (dd, J = 8.92 Hz, 2H), 5.71 (d, J = 8.92 Hz, 2H), 6.98 (d, J = 8.12 Hz, 4H), 7.04 (d, J = 1.80, 4H), 7.05 (s, 2H), 7.08 (d, J = 8.12 Hz, 2H), 7.14 (dd, J = 8.34 Hz, 25.70 Hz, 8H), 7.55 (d, J = 7.94 Hz, 2H), 7.94 (t, J = 5.5 Hz, 2H). ¹³C NMR (DMSO-*d*₆, 150 MHz) δ : 14.6, 14.8, 29.5, 31.4, 35.3, 35.4, 39.0, 46.8, 49.0, 60.2, 64.1, 68.4, 69.4, 109.8, 117.6, 127.9, 128.0, 128.9, 129.2, 129.6, 130.1, 130.8, 131.8, 131.9, 137.0, 144.7, 155.1, 155.8, 156.6, 163.6, 164.7, 167.7. HRMS m/z Calcd. for C₇₄H₈₅Cl₄N₁₀O₁₀ [M+H]⁺ 1412.5126, Found 1412.5115. HPLC purity: 95.0%.

4.1.10. *N,N'*-(Oxybis(ethane-2,1-diyl))bis(2-(4-(2-(4-(tert-butyl)-2-ethoxyphenyl)-cis-4,5-bis(4-chlorophenyl)-4,5-dihydro-1H-imidazole-1-carbonyl)-2-oxopiperazin-1-yl)acetamide) (**11c**)

¹H NMR (DMSO-*d*₆, 600 MHz) δ : 1.28 (t, J = 6.74 Hz, 6H), 1.32 (s, 18H), 2.86 (s, 4H), 3.16–3.22 (m, 6H), 3.36 (t, J = 6.21 Hz, 6H), 3.60 (d, J = 17.37 Hz, 2H), 3.67–3.72 (m, 4H), 3.81 (d, J = 16.08 Hz, 2H), 4.03–4.13 (m, 4H), 5.61 (d, J = 9.84 Hz, 2H), 5.70 (d, J = 9.84 Hz, 2H), 6.98 (d, J = 8.04 Hz, 4H), 7.04 (d, J = 8.30 Hz, 6H), 7.09 (d, J = 8.56 Hz, 2H), 7.10 (d, J = 8.69 Hz, 4H), 7.15 (d, J = 8.43 Hz, 4H), 7.55 (d, J = 7.78 Hz, 2H), 7.90 (t, J = 5.45 Hz, 2H). ¹³C NMR (DMSO-*d*₆, 150 MHz) δ : 14.8, 31.4, 35.4, 38.9, 42.7, 46.9, 49.0, 49.3, 64.1, 68.4, 69.1, 71.5, 109.3, 117.6, 117.8, 127.9, 128.0, 129.2, 130.1, 130.8, 131.6, 131.8, 136.7, 137.7, 154.8, 155.8, 156.6, 160.4, 164.8, 167.7. HRMS m/z Calcd. for C₇₂H₈₁Cl₄N₁₀O₉ [M+H]⁺ 1369.4937, Found 1369.4931. HPLC purity: 96.1%.

4.2. *In vitro* antitumor assay

A549 cells were placed in 96-well plates with 6.0 × 10³ cells in each well and subsequently incubated for 24 h in a moist atmosphere of 5% CO₂ and 37 °C. Then, different concentrations of test compounds or vehicle were added to triplicate wells. After incubation for an additional 72 h, 10% of CCK-8 in 100 μL final volume of culture medium was added to every well, then the plates were incubated for 0.5–2.0 h. The absorbance (OD value) was read at 450 nm on a spectrophotometer (Biotek Synergy H2). The values of IC₅₀ were calculated by the Logit method. All experimental results were measured in parallel three times.

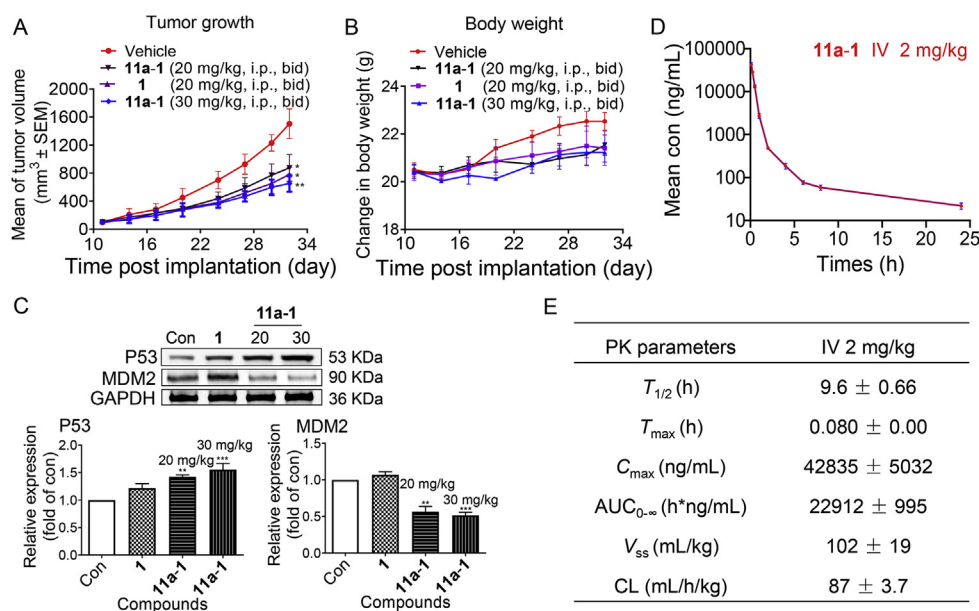


Figure 5 *In vivo* antitumor efficacy of **11a-1**. (A) Antitumor activity of compound **11a-1** in the A549 xenograft nude mouse model. Mice were treated with compound **11a-1** *via* intraperitoneal injection at 20 or 30 mg/kg twice daily for 21 continuous days. Mice were also treated with compound **1** *via* intraperitoneal injection at 20 mg/kg twice daily for 21 continuous days. The data are represented by the mean ± standard error of the mean (SEM). Significant difference was determined by one-way analysis of variance (ANOVA) test; * $P < 0.05$ and ** $P < 0.01$. (B) The body weight changes of mice during the treatment period. (C) Analysis of MDM2 and P53 induced by **11a-1** using Western blotting. Treatment with compounds **11a-1** and **1**, induced the degradation of MDM2 after 21 days at different concentrations.

4.3. Immunoblotting assay

A549 cells were cultured (3.5×10^5 cells/well) in a 6-well transparent plate for 24 h. Different concentrations of test compounds and vehicle were added to the A549 cells in the plates, and then, the plates were incubated for another 12 or 24 h. The cells were subsequently washed with cold PBS and 70 μ L of cold lysis RIPA buffer containing protease inhibitors and phosphatase inhibitors for 15 min. After placing the 6-well plate on ice for 15 min, the cells were scraped off from the plate and centrifuged at 12,000 rpm at 4 °C to collect the protein lysate. Then the lysate concentrations were tested by protein test assay. The protein extract was denatured and separated onto a 10%–15% SDS-PAGE gels.

The protein in the gels was electrotransferred onto a polyvinylidene difluoride (PVDF) membrane (Millipore). The PVDF membrane containing the proteins was rinsed with Tris-buffered saline (TBS) containing 0.1% Tween-20 (TBST) for 2 min, then blocked with 5% bovine serum albumin (BSA) buffer at room temperature for 1.5 h. The blocking solution was removed by aspiration, and the diluted primary antibody was immediately added. The membrane was incubated overnight at 4 °C. After recovering the primary antibody solution, the PVDF membrane was washed 3 times with TBST, for 5 min per time. Then, the secondary antibody was added to the membrane, which was incubated at room temperature for 1.5 h in the dark. After recovering the secondary antibody, the PVDF membrane was washed 3 times with TBST, for 5 min per time. The blot was scanned using the LI-COR Odyssey imaging system. Taking vehicle control as the standard, the expression level of protein was quantified by analysis of the gray values of the band in the obtained image. The antibodies of Western blotting were: MDM2 (Abcam, ab16895), P53 (Abcam, ab26), GAPDH (Abcam, ab8245), and secondary antibody (Abcam, ab150115).

4.4. Apoptosis assay

A549 cells with a density of 4.0×10^5 cells/well were placed in 6-well transparent plates and then treated with test compounds and vehicle in a moist atmosphere of 5% CO₂ at 37 °C for 48 h. The A549 cells were collected by trypsinization without EDTA and washed with pre-cold PBS. A549 cells were resuspended with 200 μ L of 1 × binding buffer after centrifugation and removal the supernatants. Annexin V-fluorescein isothiocyanate (FITC, 5 μ L) was added to the resuspended cell solution, which was then incubated for 15 min at room temperature. After adding 10 μ L PI, the treated cells were incubated for another 15 min in the dark at room temperature. The analysis of stained cells was performed by a flow cytometer (BD Accuri C6, USA).

4.5. *In vivo* A549 xenograft assay

The animal experiments procedures, animal use, and animal care were approved through the Animals of Committee on Ethical Use of Second Military Medical University. The *in vivo* antitumor activity was evaluated by A549 tumor xenograft by subcutaneously injecting A549 cells (5.0×10^6 cells/animal) into the flank of the BALB/c nude female mice with an average weight of 18–20 g (certificate SCXK-2007-0005, 6–7 weeks old, Shanghai Experimental Animal Center). The mice were randomized into four groups (5 mice per group) when the tumor volumes reached an average value of 100 mm³. Three treatment groups were continuously treated for 21 days with compounds **11a-1** (20 or 30 mg/kg, twice daily) and **1** (20 mg/kg, twice daily), which were administered by intraperitoneal injection. The vehicle control group was treated with an equal volume of normal saline. Tumor volumes were measured every three days with a vernier caliper, and the body weight of every mouse was recorded at in the meantime. The

volume of tumor was determined by the length and width of the tumor tissue. Eq. (1) is used to calculate the tumor volume:

$$V (\text{mm}^3) = (A \times B^2) / 2 \quad (1)$$

where A and B represent length and width of the tumor tissues, respectively. The antitumor efficacy is represented by TGI as Eq. (2):

$$\text{TGI} (\%) = (1 - V_{\text{Treat}} / V_{\text{Control}}) \times 100 \quad (2)$$

Analysis of the data was performed by one-way ANOVA test. Statistical significance was considered at $P < 0.05$.

Acknowledgments

This work was supported by National Natural Science Foundation of China (Grant Nos. 82030105, 21738002 and 21807113), the National Key R&D Program of China (Grant No. 2020YFA0509100), and the Innovation Program of Shanghai Municipal Education Commission (Grant No. 2019-01-07-00-07-E00073, China).

Author contributions

Shipeng He designed and completed most biological and cell-based assays. Junhui Ma designed and synthesized most of the target compounds. Yuxin Fang, Ying Liu and Shanchao Wu participated in research design and conducted experiments. Guoqiang Dong, Wei Wang and Chunquan Sheng proposed the project, performed data analysis and contributed to the writing—review&editing of the manuscript. All authors have given approval to the final version of the manuscript.

Conflicts of interest

There are no conflicts to declare.

Appendix A. Supporting information

Supporting data to this article can be found online at <https://doi.org/10.1016/j.apsb.2020.11.022>.

References

- Vogelstein B, Lane D, Levine AJ. Surfing the P53 network. *Nature* 2000;**408**:307–10.
- Hainaut P, Hollstein M. P53 and human cancer: The first ten thousand mutations. *Adv Cancer Res* 2000;**77**:81–137.
- Momand J, Wu HH, Dasgupta G. MDM2-master regulator of the P53 tumor suppressor protein. *Gene* 2000;**242**:15–29.
- Perry ME. The regulation of the P53-mediated stress response by MDM2 and MDM4. *Cold Spring Harb Perspect Biol* 2010;**2**:a000968.
- Vassilev LT, Vu BT, Graves B, Carvajal D, Podlaski F, Filipovic Z, et al. *In vivo* activation of the P53 pathway by small-molecule antagonists of MDM2. *Science* 2004;**303**:844–8.
- Hines J, Lartigue S, Dong H, Qian Y, Crews CM. MDM2-recruiting PROTAC offers superior, synergistic antiproliferative activity via simultaneous degradation of BRD4 and stabilization of P53. *Cancer Res* 2019;**79**:251–62.
- Wurz RP, Cee VJ. Targeted degradation of MDM2 as a new approach to improve the efficacy of MDM2–P53 inhibitors. *J Med Chem* 2019;**62**:445–7.
- Wang B, Wu S, Liu J, Yang K, Xie H, Tang W. Development of selective small molecule MDM2 degraders based on nutlin. *Eur J Med Chem* 2019;**176**:476–91.
- Wang S, Zhao Y, Aguilar A, Bernard D, Yang CY. Targeting the MDM2–P53 protein–protein interaction for new cancer therapy: Progress and challenges. *Cold Spring Harb Perspect Med* 2017;**7**:a026245.
- Zhao Y, Aguilar A, Bernard D, Wang S. Small-molecule inhibitors of the MDM2–P53 protein–protein interaction (MDM2 inhibitors) in clinical trials for cancer treatment. *J Med Chem* 2015;**58**:1038–52.
- Iancu-Rubin C, Mosoyan G, Glenn K, Gordon RE, Nichols GL, Hoffman R. Activation of P53 by the MDM2 inhibitor RG7112 impairs thrombopoiesis. *Exp Hematol* 2014;**42**:137–45. e5.
- Wagner AJ, Banerji U, Mahipal A, Somaiah N, Hirsch H, Fancourt C, et al. Phase I trial of the human double minute 2 inhibitor MK-8242 in patients with advanced solid tumors. *J Clin Oncol* 2017;**35**:1304–11.
- Lai AC, Crews CM. Induced protein degradation: an emerging drug discovery paradigm. *Nat Rev Drug Discov* 2017;**16**:101–14.
- Buckley DL, Crews CM. Small-molecule control of intracellular protein levels through modulation of the ubiquitin proteasome system. *Angew Chem Int Ed Engl* 2014;**53**:2312–30.
- Crews CM. Inducing protein degradation as a therapeutic strategy. *J Med Chem* 2018;**61**:403–4.
- Paiva SL, Crews CM. Targeted protein degradation: Elements of PROTAC design. *Curr Opin Chem Biol* 2019;**50**:111–9.
- Schapiro M, Calabrese MF, Bullock AN, Crews CM. Targeted protein degradation: Expanding the toolbox. *Nat Rev Drug Discov* 2019;**18**:949–63.
- Gao H, Sun X, Rao Y. PROTAC technology: Opportunities and challenges. *ACS Med Chem Lett* 2020;**11**:237–40.
- Wang Y, Jiang X, Feng F, Liu W, Sun H. Degradation of proteins by PROTACs and other strategies. *Acta Pharm Sin B* 2020;**10**:207–38.
- Gao H, Zheng C, Du J, Wu Y, Sun Y, Han C, et al. FAK-targeting PROTAC as a chemical tool for the investigation of non-enzymatic FAK function in mice. *Protein Cell* 2020;**11**:534–9.
- Xiang H, Zhang J, Lin C, Zhang L, Liu B, Ouyang L. Targeting autophagy-related protein kinases for potential therapeutic purpose. *Acta Pharm Sin B* 2020;**10**:569–81.
- Yang Y, Gao H, Sun X, Sun Y, Qiu Y, Weng Q, et al. Global PROTAC toolbox for degrading BCR-ABL overcomes drug-resistant mutants and adverse effects. *J Med Chem* 2020;**63**:8567–83.
- Zhou B, Hu J, Xu F, Chen Z, Bai L, Fernandez-Salas E, et al. Discovery of a small-molecule degrader of bromodomain and extra-terminal (BET) proteins with picomolar cellular potencies and capable of achieving tumor regression. *J Med Chem* 2018;**61**:462–81.
- Fulda S, Vucic D. Targeting IAP proteins for therapeutic intervention in cancer. *Nat Rev Drug Discov* 2012;**11**:109–24.
- Neklesa T, Snyder LB, Willard RR, Vitale N, Pizzano J, Gordon DA, et al. ARV-110: An oral androgen receptor PROTAC degrader for prostate cancer. *J Clin Oncol* 2019;**37**(7 Suppl):259.
- Flanagan JJ, Qian Y, Gough SM, Andreoli M, Bookbinder M, Cadelina G, et al. ARV-471, an oral estrogen receptor PROTAC degrader for breast cancer. In: Proceedings of the 2018 San Antonio Breast Cancer Symposium; 2018 Dec 4–8; San Antonio, TX. Philadelphia (PA): AACR. *Cancer Res* 2019;**79** (4 Suppl):Abstract nr P5-04-18.
- Fang Y, Liao G, Yu B. Small-molecule MDM2/X inhibitors and PROTAC degraders for cancer therapy: Advances and perspectives. *Acta Pharm Sin B* 2020;**10**:1253–78.
- Li Y, Yang J, Aguilar A, McEachern D, Przybranowski S, Liu L, et al. Discovery of MD-224 as a first-in-class, highly potent, and efficacious proteolysis targeting chimera murine double minute 2 degrader capable of achieving complete and durable tumor regression. *J Med Chem* 2019;**62**:448–66.
- Senft D, Qi J, Ronai ZA. Ubiquitin ligases in oncogenic transformation and cancer therapy. *Nat Rev Cancer* 2018;**18**:69–88.

30. Savitski MM, Zinn N, Faelth-Savitski M, Poeckel D, Gade S, Becher I, et al. Multiplexed proteome dynamics profiling reveals mechanisms controlling protein homeostasis. *Cell* 2018;**173**:260–74. e25.
31. Nabet B, Roberts JM, Buckley DL, Paulk J, Dastjerdi S, Yang A, et al. The dTAG system for immediate and target-specific protein degradation. *Nat Chem Biol* 2018;**14**:431–41.
32. Ishoey M, Chorn S, Singh N, Jaeger MG, Brand M, Paulk J, et al. Translation termination factor GSPT1 is a phenotypically relevant off-target of heterobifunctional phthalimide degraders. *ACS Chem Biol* 2018;**13**:553–60.
33. Arkin MR, Wells JA. Small-molecule inhibitors of protein–protein interactions: progressing towards the dream. *Nat Rev Drug Discov* 2004;**3**:301–17.
34. Wells JA, McClendon CL. Reaching for high-hanging fruit in drug discovery at protein–protein interfaces. *Nature* 2007;**450**:1001–9.
35. Maniaci C, Hughes SJ, Testa A, Chen W, Lamont DJ, Rocha S, et al. Homo-PROTACs: Bivalent small-molecule dimerizers of the VHL E3 ubiquitin ligase to induce self-degradation. *Nat Commun* 2017;**8**: 830.
36. Lindner S, Steinebach C, Kehm H, Mangold M, Gutschow M, Kronke J. Chemical inactivation of the E3 ubiquitin ligase cereblon by pomalidomide-based homo-PROTACs. *J Vis Exp* 2019;(147): e59472.
37. Steinebach C, Kehm H, Lindner S, Vu LP, Kopff S, Lopez Marmol A, et al. PROTAC-mediated crosstalk between E3 ligases. *Chem Commun* 2019;**55**:1821–4.
38. Zhuang C, Miao Z, Wu Y, Guo Z, Li J, Yao J, et al. Double-edged swords as cancer therapeutics: Novel, orally active, small molecules simultaneously inhibit P53–MDM2 interaction and the NF-kappaB pathway. *J Med Chem* 2014;**57**:567–77.
39. Dong G, He S, Qin X, Liu T, Jiang Y, Li X, et al. Discovery of nonpeptide, environmentally sensitive fluorescent probes for imaging P53–MDM2 interactions in living cell lines and tissue slice. *Anal Chem* 2020;**92**:2642–8.
40. Wang S, Jiang Y, Wu S, Dong G, Miao Z, Zhang W, et al. Meeting organocatalysis with drug discovery: Asymmetric synthesis of 3,3'-spirooxindoles fused with tetrahydrothiopyrans as novel P53-MDM2 inhibitors. *Org Lett* 2016;**18**:1028–31.
41. Zhuang C, Miao Z, Zhu L, Dong G, Guo Z, Wang S, et al. Discovery, synthesis, and biological evaluation of orally active pyrrolidone derivatives as novel inhibitors of P53–MDM2 protein–protein interaction. *J Med Chem* 2012;**55**:9630–42.
42. He S, Dong G, Wu S, Fang K, Miao Z, Wang W, et al. Small molecules simultaneously inhibiting P53–murine double minute 2 (MDM2) interaction and histone deacetylases (HDACs): Discovery of novel multi-targeting antitumor agents. *J Med Chem* 2018;**61**:7245–60.
43. Yang J, Li Y, Aguilar A, Liu Z, Yang CY, Wang S. Simple structural modifications converting a bona fide MDM2 PROTAC degrader into a molecular glue molecule: A cautionary tale in the design of PROTAC degraders. *J Med Chem* 2019;**62**:9471–87.
44. Lu Q, Ding X, Huang T, Zhang S, Li Y, Xu L, et al. BRD4 degrader ARV-825 produces long-lasting loss of BRD4 protein and exhibits potent efficacy against cholangiocarcinoma cells. *Am J Transl Res* 2019;**11**:5728–39.
45. Liu J, Chen H, Ma L, He Z, Wang D, Liu Y, et al. Light-induced control of protein destruction by opto-PROTAC. *Sci Adv* 2020;**6**: eaay5154.
46. Duan L, Perez RE, Chen L, Blatter LA, Maki CG. P53 promotes AKT and SP1-dependent metabolism through the pentose phosphate pathway that inhibits apoptosis in response to Nutlin-3a. *J Mol Cell Biol* 2018;**10**:331–40.